SOLAR PHYSICS

Global maps of the magnetic field in the solar corona

Zihao Yang[1], Christian Bethge[2,3], Hui Tian[1,4]*, Steven Tomczyk[3]*, Richard Morton[5], Giulio Del Zanna[6], Scott W. McIntosh[3], Bidya Binay Karak[7], Sarah Gibson[3], Tanmoy Samanta[8,9], Jiansen He[1], Yajie Chen[1,10], Linghua Wang[1]

Understanding many physical processes in the solar atmosphere requires determination of the magnetic field in each atmospheric layer. However, direct measurements of the magnetic field in the Sun's corona are difficult to obtain. Using observations with the Coronal Multi-channel Polarimeter, we have determined the spatial distribution of the plasma density in the corona and the phase speed of the prevailing transverse magnetohydrodynamic waves within the plasma. We combined these measurements to map the plane-of-sky component of the global coronal magnetic field. The derived field strengths in the corona, from 1.05 to 1.35 solar radii, are mostly 1 to 4 gauss. Our results demonstrate the capability of imaging spectroscopy in coronal magnetic field diagnostics.

The solar atmosphere is shaped by its magnetic field. Because of magnetic coupling between the various atmospheric layers, understanding many physical processes in the solar atmosphere requires information on the magnetic field of the whole atmosphere. However, only limited measurements are available for the magnetic field in the upper solar atmosphere, especially in the outermost atmospheric layer, the corona (*1*).

Information on the magnetic field at the solar surface is usually obtained through the Zeeman effect, the splitting of spectral lines in the presence of a magnetic field. However, it is difficult to use this method to measure the coronal magnetic field, mainly because of the negligible line splitting induced by the much weaker magnetic field in the corona. A few attempts have been made to measure the coronal magnetic field using the Zeeman effect, but only in small regions where a strong field is present (*2*, *3*). Spectro-polarimetric measurements can also determine the local coronal magnetic field in some cool loop–like structures or prominences (e.g., *4*, *5*). Coronal magnetic field strengths can be inferred from observations of waves and oscillations, although most previous studies only provided an estimate of the average field strengths in individual oscillating structures (e.g., *6*–*9*). Observations of shocks driven by solar eruptions can also be used to infer coronal magnetic field strengths along the shock paths (e.g., *10*, *11*) but such shocks are only occasionally observed. Radio observations have also been used to estimate the coronal magnetic field but only in localized regions (e.g., *12*, *13*); this method often requires accurate identification of the radio-emission mechanisms, which are not always clear. Because of the observational difficulties with each of these methods, no routine measurements of the global coronal magnetic field are available.

We used the Coronal Multi-channel Polarimeter (CoMP) (*14*) to observe the corona outside the whole disk of the Sun on 14 October 2016. The CoMP data included spectral profiles of the Fe XIII lines at 1074.7 and 1079.8 nm in the corona from 1.05 to 1.35 solar radii (*15*). We fitted each line profile with a gaussian function to obtain the line intensity and Doppler velocity at each pixel within the CoMP field of view (FOV) (*16*). Figure 1, B and C, shows the intensity images of these two lines averaged over the period of 19:24 to 20:17 UT. For comparison, Fig. 1A shows a simultaneous coronal image in the Fe XII 19.3-nm channel of the Atmospheric Imaging Assembly (AIA) (*17*) on the Solar Dynamics Observatory (SDO) spacecraft. The intensity ratio of the two Fe XIII lines (Fig. 1D) is sensitive to the electron density, allowing us to derive (*15*) a global map of the coronal electron density (Fig. 1E). The measured electron number density is mostly in the range of $10^{7.5}$ to $10^{8.5}$ cm^{-3}. The associated uncertainties, which arise from both the statistical measurement uncertainties and the systematic uncertainties in the atomic physics parameters used to calculate the relationship between electron density and line ratio (*15*), were mostly 10 to 25% (Fig. 1F). Assuming a standard coronal elemental abundance and electrical neutrality, the corresponding total mass density (ρ) was calculated as $\rho = 1.2 N_e m_P$, where m_P is the mass of a proton (*18*).

Previous CoMP observations have found propagating periodic disturbances in the Doppler velocity of Fe XIII 1074.7 nm, indicating the ubiquitous presence of transverse magnetohydrodynamic (MHD) waves in the corona (e.g., *19*-*22*). A wave-tracking technique has previously been developed to track the propagation of the Doppler velocity perturbation and to calculate the phase speed of the transverse wave along its propagation path (*20*). Similarly pervasive velocity fluctuations also appear in our dataset (movie S1). We applied a modified version of the wave-tracking technique (*15*) to the Doppler velocity image sequence of Fe XIII 1074.7 nm during the time period of 20:39 to 21:26 UT and calculated the wave phase speed and measurement uncertainty (*15*) at each pixel within the FOV (Fig. 2). The phase speed mostly fell in the range of 300 to 700 km s^{-1}, and the associated uncertainty was generally smaller than 40 km s^{-1}.

We identified the observed transverse MHD waves as kink waves, which have an Alfvénic nature (e.g., *8*, *23*-*26*). The phase speed (kink speed), c_k, can be expressed as follows (*27*):

$$c_k^2 = \frac{B_i^2 + B_o^2}{\mu_0(\rho_i + \rho_o)} \quad (1)$$

where μ_0 is the magnetic permeability of a vacuum, B is the magnetic field strength, ρ is the mass density, and the subscripts i and o indicate physical parameters inside and outside the wave-guiding magnetic field structures (flux tubes), respectively. In the coronal plasma environment, the pressure balance across flux tubes is dominated by the magnetic pressure, so $B_i \sim B_o$ [see, e.g., (*20*), (*21*), and (*26*)]. Because individual flux tubes are likely unresolved at the spatial resolution of CoMP (~7000 km), we used the density averaged inside and outside flux tubes (ρ) within each spatial pixel and estimated the magnetic field strength using the following equation (*21*, *26*, *28*):

$$c_k = \frac{B}{\sqrt{\mu_0 \rho}} \quad (2)$$

Our measurements are based on spectral profiles that result from an integration of the spectral line emissivity (the released energy per unit time per unit volume during an electron transition from a higher energy level to a lower one, increasing with density) along the line of sight (LOS). The derived density, phase speed, and magnetic field strength are therefore all weighted by the emissivity along the LOS. Because the density generally decreases with distance from the solar limb, LOS weighting favors magnetic structures in the vicinity of the plane of sky (POS), i.e., the plane passing through the center of the Sun and perpendicular to the LOS. We expect the phase speed measured from the data to correspond to the kink speed projected onto the POS. If we further approximate the

[1]School of Earth and Space Sciences, Peking University, Beijing 100871, People's Republic of China. [2]Universities Space Research Association, Huntsville, AL 35805, USA. [3]High Altitude Observatory, National Center for Atmospheric Research, Boulder, CO 80307, USA. [4]Key Laboratory of Solar Activity, National Astronomical Observatories, Chinese Academy of Sciences, Beijing 100012, People's Republic of China. [5]Department of Mathematics, Physics and Electrical Engineering, Northumbria University, Newcastle Upon Tyne NE1 8ST, UK. [6]Department of Applied Mathematics and Theoretical Physics, Centre for Mathematical Sciences, University of Cambridge, Cambridge CB3 0WA, UK. [7]Department of Physics, Indian Institute of Technology (Banaras Hindu University), Varanasi 221005, India. [8]Department of Physics and Astronomy, George Mason University, Fairfax, VA 22030, USA. [9]Johns Hopkins University Applied Physics Laboratory, Laurel, MD 20723, USA. [10]Max Planck Institute for Solar System Research, 37077 Göttingen, Germany.
*Corresponding author. Email: huitian@pku.edu.cn (H.T.); tomczyk@ucar.edu (S.T.)

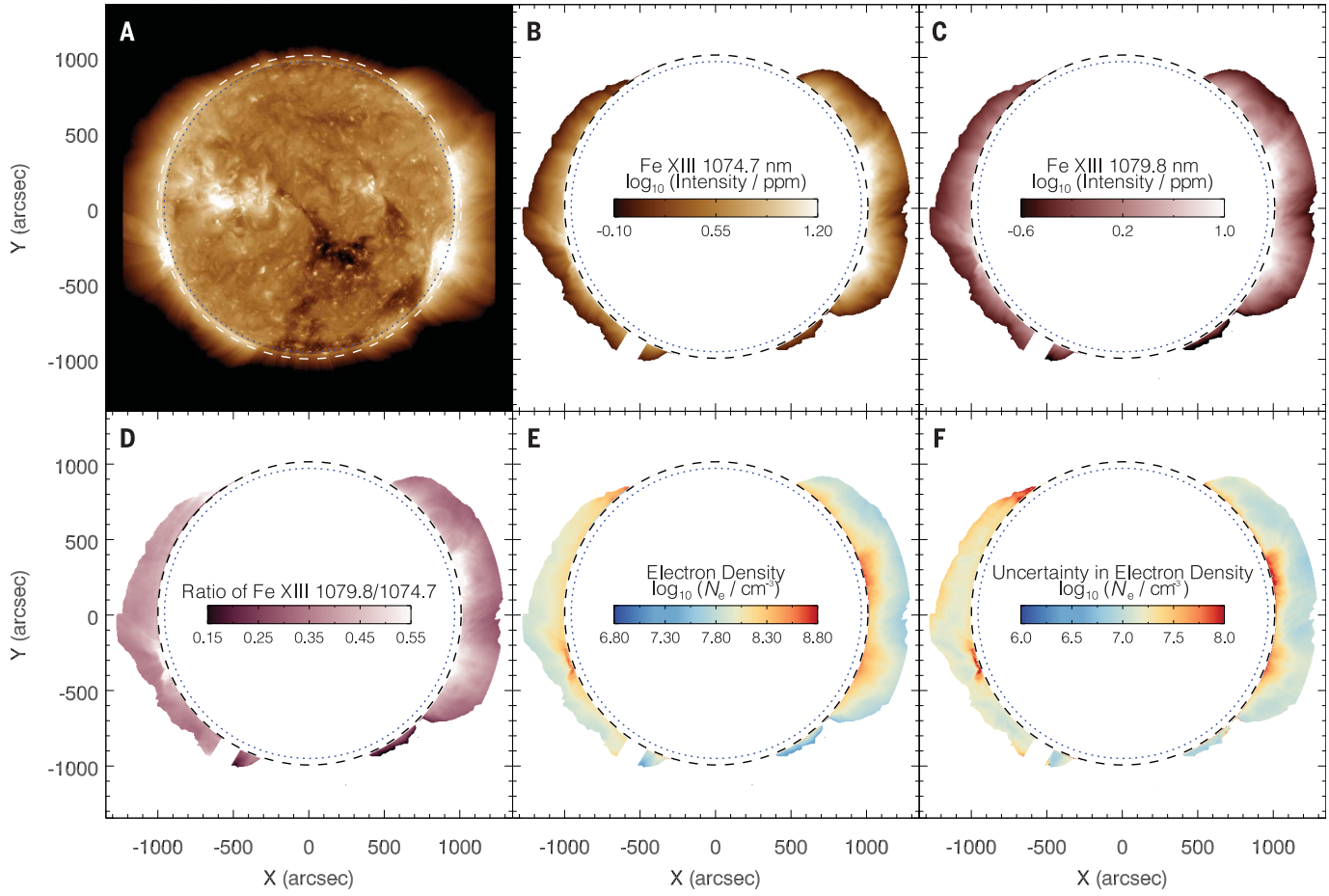

Fig. 1. Images of the solar corona and density diagnostic results. (**A**) AIA 19.3-nm intensity image taken at 19:25:55 UT on 14 October 2016. (**B** and **C**) CoMP Fe XIII 1074.7-nm and 1079.8-nm peak intensity images averaged over the time period of 19:24 to 20:17 UT on 14 October 2016 expressed as parts per million (ppm) of the solar disk intensity and plotted on a logarithmic color scale. (**D**) Map of the 1079.8-nm/1074.7-nm intensity ratio. (**E** and **F**) Maps of the derived electron density and associated uncertainty. In all panels, the dotted circle marks the edge of the solar disk (limb) and the dashed circle indicates the inner boundary of the CoMP FOV. The *x* and *y* coordinates are positions in the east–west and south–north directions, respectively, measured from the center of the solar disk.

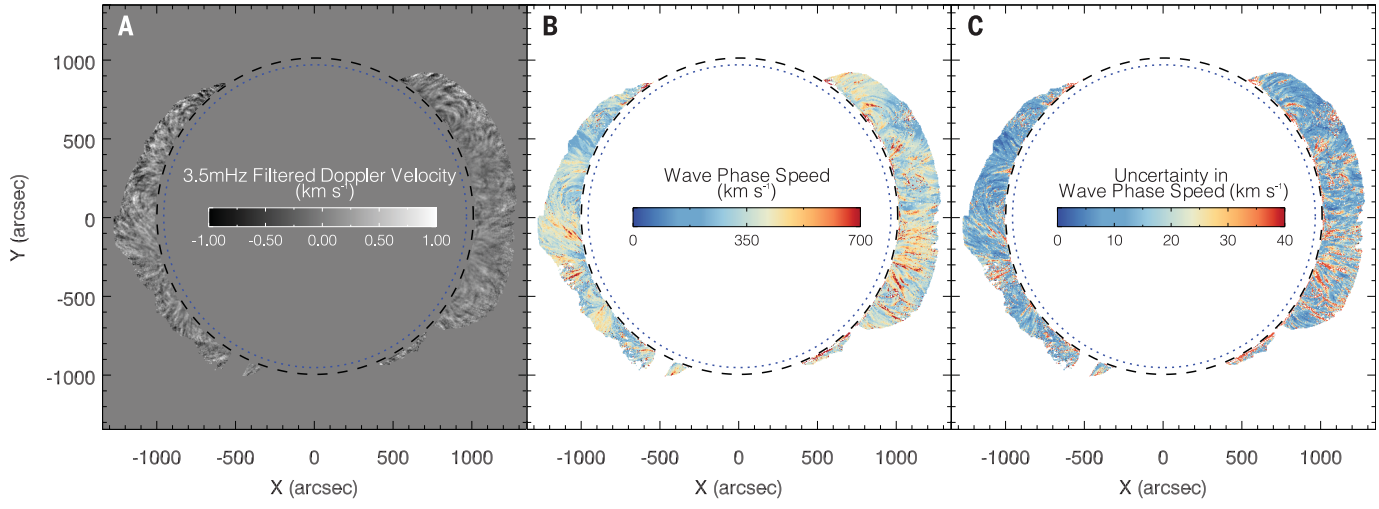

Fig. 2. Doppler velocity and wave-tracking results. (**A**) Map of the Doppler velocity of the Fe XIII 1074.7-nm line at 20:39:09 UT. A 3.5-mHz gaussian filter has been applied to the Doppler shift image sequence (*15*). Movie S1 shows an animated version of this panel. (**B** and **C**) Maps of the derived wave phase speed and associated uncertainty. The circles are as in Fig. 1.

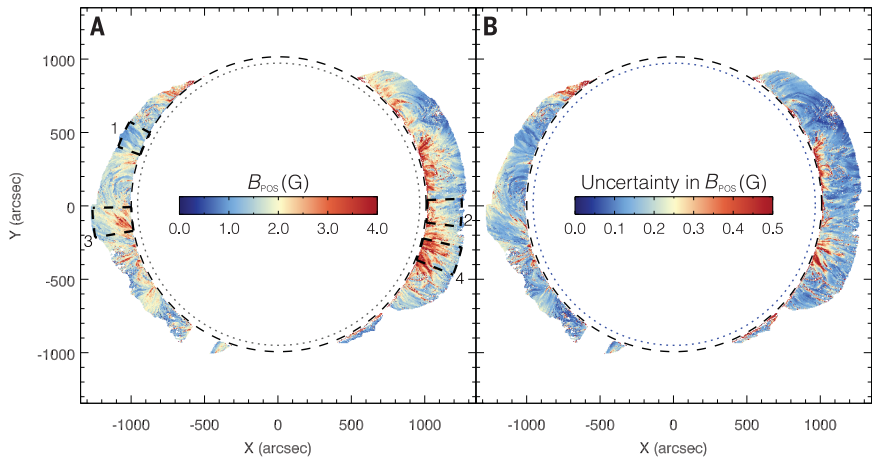

Fig. 3. Maps of the coronal magnetic field derived from observations. (**A**) Map of B_{POS}. The four numbered black annulus sectors indicate the regions used for Fig. 4, C to F. (**B**) Map of the associated uncertainty. The circles are as in Fig. 1.

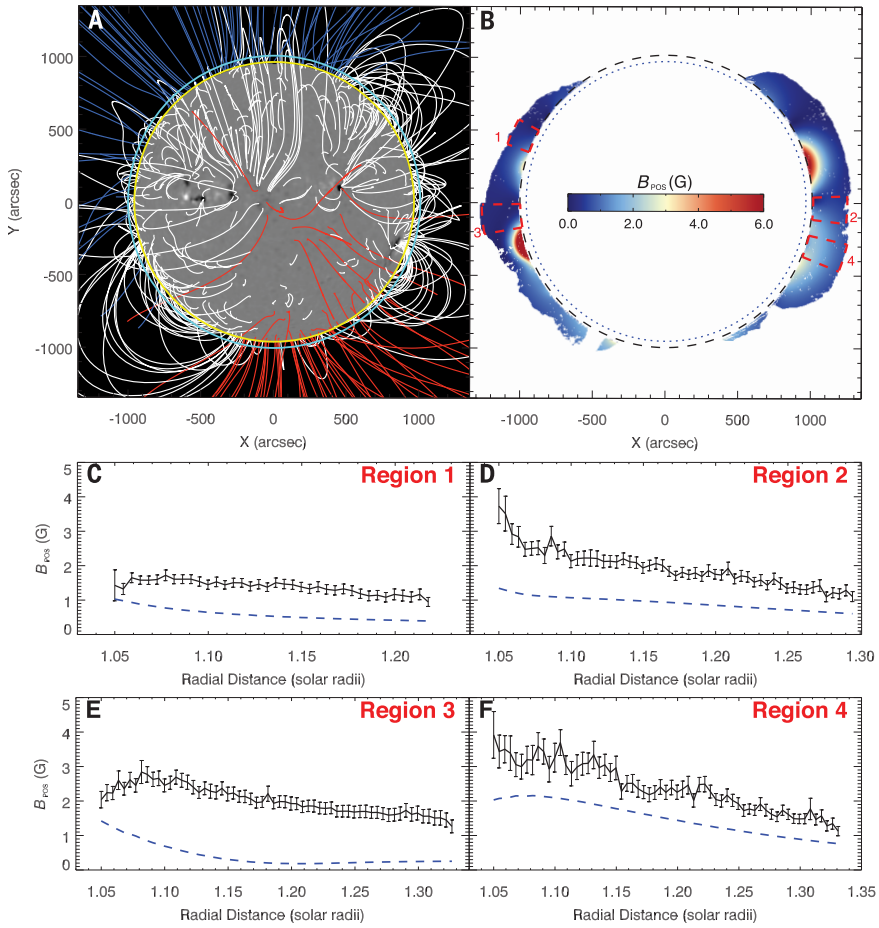

Fig. 4. Comparison between the coronal magnetic field derived from observations and that extrapolated using the PFSS model. (**A**) PFSS model field lines overlain on a photospheric synoptic magnetogram (*15*) reconstructed using HMI observations from the SDO. The magnetogram and model field lines sampled at 18:03:28 UT have been rotated and are shown from the Earth's viewpoint at 20:39:09 UT. The yellow and cyan circles mark the solar limb and the inner boundary of the CoMP FOV, respectively. The white lines are closed field lines, and the red and blue lines represent open field lines with opposite polarities. (**B**) Same as Fig. 3A but showing the map of B_{POS} generated from the PFSS model. (**C** to **F**) Average magnetic field strengths as a function of radial distance from the solar center for the four sectors marked in (B) and in Fig. 3A. The black solid lines with error bars are B_{POS} derived from the observations and associated uncertainties, and the blue dashed lines show B_{POS} calculated from the PFSS model.

average density in the vicinity of the POS with the derived density, we can obtain the POS component of the coronal magnetic field strength (B_{POS}) using Eq. 2. Forward simulations of propagating Alfvénic waves have shown that this is an appropriate approximation (*28*).

Our derived global coronal magnetic field map and its uncertainty are shown in Fig. 3. Comparing Fig. 3A with the intensity images in Fig. 1, A to C, shows that the magnetic field is higher in regions with stronger coronal emission. Typical values of B_{POS} in the FOV are 1 to 4 gauss, similar to the magnetic field strengths in smaller coronal regions inferred using other methods (*3*, *10*, *11*). The uncertainties in B_{POS}, which we calculated by propagating the uncertainties in the measured density and phase speed (*15*), are shown in Fig. 3B and are generally smaller than 15%. There could be an additional uncertainty caused by our use of the POS emissivity instead of the LOS-integrated emissivity in the calculation of the theoretical relationship between line ratio and electron density. Because the electron density distribution along the LOS is unknown, we estimated the impact of this assumption using a model of homogeneous density distribution with spherical symmetry (*15*). The density estimated with our line ratio method was lower than the local density in the POS (from the density model) by ~30%. Following Eq. 2, this corresponds to a possible additional uncertainty of ~12% on the measured B_{POS}.

In the absence of routine measurements of the coronal magnetic field, the potential field source surface (PFSS) model (*15*, *29*) is often adopted to extrapolate the observed magnetic field on the solar surface to the corona. For comparison with our method, we also used the PFSS model to reconstruct the three-dimensional coronal magnetic field structures from observations of the Helioseismic and Magnetic Imager (HMI) (*30*) on SDO (Fig. 4A) and obtain a map of B_{POS} from the model (*15*) (Fig. 4B). A comparison between the map of B_{POS} extrapolated using the PFSS model and that estimated from our data shows similar distributions of coronal magnetic field on the global scale but differences at scales smaller than ~200 arcsec. At many locations, the radial variation of B_{POS} has a discrepancy between CoMP measurements and PFSS results (Fig. 4, C to F). Some of these differences may arise because the magnitude of B_{POS} from the PFSS model is plotted for a POS slice. The B_{POS} derived from our CoMP data represents a measurement weighted by the emissivity along the LOS and is the POS component of the magnetic field strength averaged inside and outside flux tubes. We nevertheless compared the two B_{POS} maps because the LOS weighting favors magnetic structures in the vicinity of the POS. Differences between the two B_{POS} maps could also be related to the assumptions used in the PFSS model (*15*).

Our method for measuring the coronal magnetic field requires a continuous observation of 1 to 2 hours under good conditions, including ~1 hour to observe the transverse waves and additional time for density diagnostics. This implicitly assumes that the coronal structures do not evolve during the observing period. We expect this to be valid in the absence of eruptive events. The technique may not be applied to regions affected by solar eruptions, where signatures of transverse waves are often masked by the rapidly changing magnetic field environment.

Subject to these assumptions and limitations, our results demonstrate that imaging spectroscopy can be used to determine the coronal magnetic field. In principle, this technique could be applied to continuous observations from CoMP-like instruments to produce routine global coronal magnetic field maps.

REFERENCES AND NOTES

1. T. Wiegelmann, J. K. Thalmann, S. K. Solanki, *Astron. Astrophys. Rev.* **22**, 78 (2014).
2. H. Lin, M. J. Penn, S. Tomczyk, *Astrophys. J.* **541**, L83–L86 (2000).
3. H. Lin, J. R. Kuhn, R. Coulter, *Astrophys. J.* **613**, L177–L180 (2004).
4. D. Kuridze *et al*., *Astrophys. J.* **874**, 126 (2019).
5. B. Schmieder *et al*., *Astron. Astrophys.* **569**, A85 (2014).
6. W. Liu *et al*., *Astrophys. J.* **736**, L13 (2011).
7. V. M. Nakariakov, L. Ofman, *Astron. Astrophys.* **372**, L53–L56 (2001).
8. H. Tian *et al*., *Astrophys. J.* **759**, 144 (2012).
9. Y. Chen *et al*., *Astrophys. J.* **728**, 147 (2011).
10. N. Gopalswamy, N. Nitta, S. Akiyama, P. Mäkelä, S. Yashiro, *Astrophys. J.* **744**, 72 (2012).
11. A. Kumari, R. Ramesh, C. Kathiravan, T. J. Wang, N. Gopalswamy, *Astrophys. J.* **881**, 24 (2019).
12. G. D. Fleishman *et al*., *Science* **367**, 278–280 (2020).
13. S. Mancuso, M. V. Garzelli, *Astron. Astrophys.* **560**, L1 (2013).
14. S. Tomczyk *et al*., *Sol. Phys.* **247**, 411–428 (2008).
15. Materials and methods are available as supplementary materials.
16. H. Tian *et al*., *Sol. Phys.* **288**, 637–650 (2013).
17. J. R. Lemen *et al*., *Sol. Phys.* **275**, 17–40 (2012).
18. E. Priest, *Solar Magnetohydrodynamics* (Springer, 1982).
19. S. Tomczyk *et al*., *Science* **317**, 1192–1196 (2007).
20. S. Tomczyk, S. W. McIntosh, *Astrophys. J.* **697**, 1384–1391 (2009).
21. R. J. Morton, S. Tomczyk, R. Pinto, *Nat. Commun.* **6**, 7813 (2015).
22. R. J. Morton, M. J. Weberg, J. A. McLaughlin, *Nat. Astron.* **3**, 223–229 (2019).
23. B. De Pontieu *et al*., *Science* **318**, 1574–1577 (2007).
24. M. Goossens, J. Terradas, J. Andries, I. Arregui, J. L. Ballester, *Astron. Astrophys.* **503**, 213–223 (2009).
25. S. W. McIntosh *et al*., *Nature* **475**, 477–480 (2011).
26. D. M. Long, G. Valori, D. Pérez-Suárez, R. J. Morton, A. M. Vásquez, *Astron. Astrophys.* **603**, A101 (2017).
27. P. M. Edwin, B. Roberts, *Sol. Phys.* **88**, 179–191 (1983).
28. N. Magyar, T. Van Doorsselaere, *Astrophys. J.* **856**, 144 (2018).
29. K. H. Schatten, J. M. Wilcox, N. F. Ness, *Sol. Phys.* **6**, 442–455 (1969).
30. P. H. Scherrer *et al*., *Sol. Phys.* **275**, 207–227 (2012).
31. Source codes for: Z. Yang, C. Bethge, H. Tian, S. Tomczyk, R. Morton, G. Del Zanna, S. W. McIntosh, B. B. Karak, S. Gibson, T. Samanta, J. He, Y. Chen, L. Wang, Global maps of the magnetic field in the solar corona, Zenodo (2020); https://doi.org/10.5281/zenodo.3884044.

ACKNOWLEDGMENTS

We thank the SDO team for providing the AIA and HMI data, M. Galloy for running the CoMP data-processing pipeline, and M. DeRosa for helpful discussion about PFSS. This material is based on work supported by the National Center for Atmospheric Research, which is a major facility sponsored by the National Science Foundation under cooperative agreement no. 1852977. The AIA and HMI are instruments on SDO, a mission of NASA's Living With a Star Program. **Funding:** This work was supported by NSFC grants 11825301, 11790304(11790300), 41421003, 41774183, 41861134033, and 41874200; the Strategic Priority Research Program of CAS (grant no. XDA17040507), the Max Planck Partner Group program, STFC (UK) through consolidated grants to the atomic astrophysics group at DAMTP at the University of Cambridge (ST/P000665/1 and ST/T000481/1); and the Department of Science and Technology (SERB/DST) through the Ramanujan Fellowship (project no. SB/S2/RJN-017/2018). **Author contributions:** H.T. led the project. S.T. developed the CoMP instrument, designed the observing sequences, and processed the raw data. Z.Y. analyzed the data and generated the figures and movies under H.T.'s guidance. H.T. and Z.Y. wrote the manuscript. C.B improved the CoMP data-processing pipeline and led the first stage of data analysis. R.M. contributed to the magnetic field determination. G.D.Z. contributed to the density estimation. S.T. and S.W.M. developed the wave-tracking method, with contributions from R.M. and B.B.K. S.G. developed the software for the calculation of POS magnetic field from the PFSS model. Y.C. assisted with the PFSS calculation. T.S., J.H., and L.W. advised on the data analysis and contributed to the interpretation of the observations. All authors have discussed the results and commented on the manuscript. **Competing interests:** The authors declare no competing interests. **Data and materials availability:** The CoMP data can be obtained at http://download.hao.ucar.edu/d5/mlso/pub/comp-continuum-correction/; we used the files that begin with 20161014. The AIA data are available at the Joint Science Operations Center (JSOC) http://jsoc.stanford.edu/AIA/AIA_lev1.html; we used the AIA 193 Å image taken at 19:25:55 UT on 14 October 2016. The HMI synoptic photospheric magnetogram and results of our PFSS model are available in hierarchical data format at https://www.lmsal.com/solarsoft/archive/ssw/pfss_links_v2/Bfield_20161014_180328.h5. Source codes for the wave tracking and density diagnostic are available at Zenodo (*31*).

SUPPLEMENTARY MATERIALS

science.sciencemag.org/content/369/6504/694/suppl/DC1
Materials and Methods
Supplementary Text
Figs. S1 to S4
References (*32*–*54*)
Movie S1

24 February 2020; accepted 10 June 2020
10.1126/science.abb4462

Global maps of the magnetic field in the solar corona

Zihao Yang, Christian Bethge, Hui Tian, Steven Tomczyk, Richard Morton, Giulio Del Zanna, Scott W. McIntosh, Bidya Binay Karak, Sarah Gibson, Tanmoy Samanta, Jiansen He, Yajie Chen and Linghua Wang

Science **369** (6504), 694-697.
DOI: 10.1126/science.abb4462

The magnetic field in the Sun's corona

The solar corona is the outermost layer of the Sun's atmosphere, consisting of hot, diffuse, and highly ionized plasma. The magnetic field in this region is expected to drive many of its physical properties but has been difficult to measure with observations. Yang *et al.* used near-infrared imaging spectroscopy to determine the electron density and magnetohydrodynamic wave speed in the corona. By combining these measurements, they derived maps of the magnetic field throughout the entire observable corona. The method could potentially be used to produce routine magnetic field maps for the corona that are similar to those already available for the Sun's surface.

Science, this issue p. 694